Optical Fiber Technology xxx (2009) xxx–xxx

Contents lists available at ScienceDirect

Optical Fiber Technology

www.elsevier.com/locate/yofte

Invited Paper

Nonlinear signal–noise interactions in dispersion-managed links with various modulation formats

Alberto Bononi *, Paolo Serena, Nicola Rossi

Universitá degli Studi di Parma, Dip. Ingegneria dell'Informazione, Viale G. Usberti 181/A, 43100 Parma, Italy

ARTICLE INFO

Article history:
Received 6 August 2009
Revised 30 October 2009
Available online xxxx

Keywords:
Dispersion management
Parametric gain
Nonlinear phase noise
Modulation formats
Coherent detection
Nonlinear threshold

ABSTRACT

Purpose of this paper is to highlight the principles of the nonlinear signal–noise interaction (NSNI) in dispersion-managed long-haul optical links and provide a quantitative understanding of the system parameters for which NSNI sets the nonlinear performance of the most popular intensity and phase modulation formats, namely on–off keying, differential binary and quadrature phase-shift keying and coherent quadrature phase-shift keying.

1. Introduction

Standard analysis by simulation of the performance of advanced modulation formats in dispersion-managed (DM) lines, as implemented in most commercially-available simulation packages, makes the simplifying assumption that amplified spontaneous emission (ASE) noise can be loaded at the receiver as a single additive white Gaussian noise process, while the signal, be it either a single-channel or a wavelength division multiplex (WDM), is propagated through the DM line using the standard split-step Fourier method (SSFM) [1]. Such a "receiver noise loading" technique allows a reduced number of SSFM propagation runs needed for bit error rate (BER) estimation:

- Only one run is needed in single-channel propagation when using a sufficiently long De Brujin sequence that captures all possible inter-symbol interference (ISI) patterns within the memory length of the DM line [2,3];
- Several runs are needed in WDM propagation in order to test different time and phase offsets among the channels, all modulated with different De Brujin sequences.

The receiver noise loading thus allows, for the usual large BER values (of the order of 10^{-3}) of DM lines with forward error correction (FEC), a reasonably fast BER estimation by direct Monte Carlo (MC) error counting. If lower BERs are of interest, one can use sophisticated pseudo-analytical BER evaluation techniques, such as the Karhunen–Loeve method for quadratic detectors in additive Gaussian noise [4], whose input is the noiseless received optical field.

Receiver noise loading provides correct performance results whenever the nonlinear signal–noise interaction (NSNI) during propagation can be neglected. When NSNI is significant, Gaussian ASE random samples must be added at each amplifier along the line and the compound signal-ASE field propagated up to the receiver. Many SSFM propagation runs with different ASE noise samples must be performed until sufficiently many errors at the receiver have been counted. MC simulations are therefore orders of magnitude slower than with noise loading.

Purpose of this paper, which is an extension of a companion paper presented at ECOC'09 [5], is to perform a systematic study by simulation of the range of DM line parameters for which NSNI is the dominant nonlinear impairment and thus cannot be neglected. In so doing we will also explore the role of other nonlinearities in comparison with NSNI.

The study will be carried out for the following popular modulation formats: on–off keying (OOK), differential binary and quaternary phase-shift keying (DPSK and DQPSK, respectively) with incoherent interferometric reception, and polarization-division-multiplexing coherent QPSK (PDM-QPSK). The schemes for the standard optical receivers that follow the channel-selection optical filter for the above formats are summarized in Fig. 1. Mach–Zehnder delay interferometers with one symbol delay T and balanced photo-detection are used for DPSK and DQPSK [6,7]. The digital-signal-processing (DSP)-based coherent receiver for PDM-QPSK [7–9] uses a polarization beam splitter to split the polarizations

* Corresponding author. Fax: +39 521 905 758.
E-mail address: bononi@tlc.unipr.it (A. Bononi).

1068-5200/$ - see front matter © 2009 Elsevier Inc. All rights reserved.
doi:10.1016/j.yofte.2009.11.001

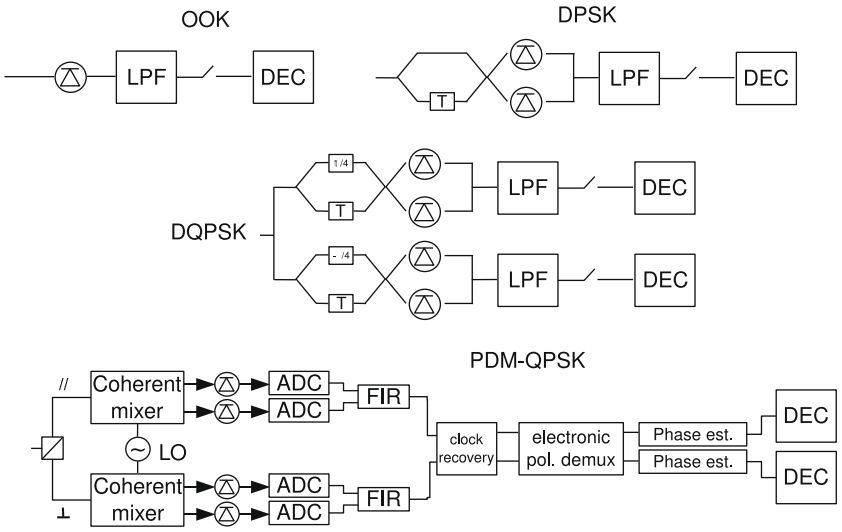

Fig. 1. Schemes of optical receivers for OOK, DPSK, DQPSK [6,7] and PDM-QPSK [8,9,7,10] formats. LPF, low-pass electrical filter; DEC, decision block; LO, local oscillator; ADC, analog–digital converter; FIR, finite impulse response digital filter for GVD compensation.

of the incoming signal, and then the local oscillator is optically mixed with the signal in two optical hybrids (coherent mixers) followed by photo-detection, analog to digital conversion (i.e., sampling), FIR filtering for electronic group-velocity dispersion (GVD) compensation. Then clock recovery follows, and then electronic polarization demultiplexing and polarization-mode dispersion (PMD) mitigation is performed, usually with a constant-modulus algorithm (CMA). Finally a frequency recovery (not shown) and an M-power law feed-forward phase recovery (sometimes also called Viterbi and Viterbi (V&V) [11] phase estimation) are performed and phase decisions are made. Clearly, the coherent receiver is way more complex than the incoherent receivers, although its ability to electrically equalize optical linear and partly nonlinear distortions, and the very selective electrical filtering it offers are key enablers for high spectral efficiency modulation formats in long-haul DM lines [12].

This paper is organized as follows. Section 2 presents a summary of the most relevant known theoretical models dealing with NSNI in DM lines. In particular, we will show that the most relevant information for performance evaluation of both amplitude and phase modulation formats is contained in the spectrum of the in-phase and quadrature ASE, and that the spectrum of phase noise is quite similar to that of the quadrature ASE. Section 3 describes the simulations set-up and techniques for the various modulation formats, and presents single-channel and WDM performance results for a long-haul terrestrial DM system in terms of Q-factor versus transmitted power, and nonlinear power threshold versus baudrate. We provide a discussion of the simulation results, with interpretations in the light of existing theoretical models. Finally, Section 5 contains our conclusions.

2. NSNI models

Following the taxonomy of nonlinear effects presented in Fig. 12 of [6], we will next consider both single-channel (or intra-channel) NSNI and wavelength division multiplexing (WDM) (or inter-channel) NSNI, and discuss some relevant available analytical models.

2.1. Single-channel NSNI

Any optical signal of sufficiently large power propagating in a long-haul fiber link interacts with the additive white Gaussian amplified spontaneous emission (ASE) noise through a four-wave mixing (FWM) process. At the end of the link, the received ASE field probability density function (PDF) changes to a bean-like non-Gaussian shape [13], while the ASE power spectral density (PSD) changes from white to colored, with a typical low-pass spectral enhancement around the signal optical carrier [1]. This NSNI is also known as parametric gain (PG) [1]. The phase of the composite signal + ASE field, after subtraction of the phase of the average field, can be thought of as the sum of a linear component that would be present even in absence of PG, and of a nonlinear extra component known as nonlinear phase noise (NLPN) [14].

As an illustrative example, we propagated with the SSFM a continuous-wave (CW) signal along a singly-periodic DM terrestrial link, sketched in Fig. 2, with $N = 20$ spans of transmission fiber with dispersion $D_{tx} = 4$ ps/nm/km, attenuation $\alpha_{\rm dB} = 0.2$ dB/km, nonlinear coefficient $\gamma = 1.4\ {\rm W}^{-1}\ {\rm km}^{-1}$, span length 100 km (in fact, any span length exceeding 50 km, i.e., much longer than the fiber attenuation length $1/\alpha$ would give the same noiseless signal distortions), per span dispersion compensation with in-line residual dispersion per span (RDPS) $D_{in} = 0$ (nonlinearities in the in-line compensating fiber are neglected), pre-compensation $D_{pre} = -85$ ps/nm, and post-compensation $D_{post} = 85$ ps/nm chosen so as to have zero net residual dispersion $D_{tot} = D_{pre} + ND_{in} + D_{post}$, a typical choice for phase-modulated formats. The transmitted CW power P_{tx} was 4.6 dBm (giving $\Phi_{CW} = N\frac{\gamma}{\alpha}P_{tx} = 0.6\pi$ [rad] of CW accumulated nonlinear phase). Gaussian ASE noise was added at each in-line amplifier, for a (linear) received optical signal-to-noise ratio (OSNR) of 12 dB over 0.1 nm (e.g., giving BER $= 10^{-5}$ in DQPSK at 10 Gbaud in the linear regime).

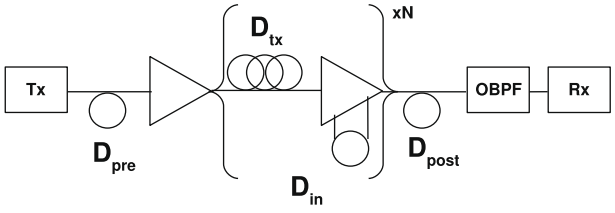

Fig. 2. DM terrestrial link with N spans, transmission fiber with dispersion D_{tx} (ps/nm/km), in-line residual dispersion per span D_{in} (ps/nm), dispersion pre-compensation D_{pre} (ps/nm) and post-compensation D_{post} (ps/nm). OBPF, optical bandpass channel-selection filter.

Please cite this article in press as: A. Bononi et al., Nonlinear signal–noise interactions in dispersion-managed links with various modulation formats, Opt. Fiber Technol. (2009), doi:10.1016/j.yofte.2009.11.001

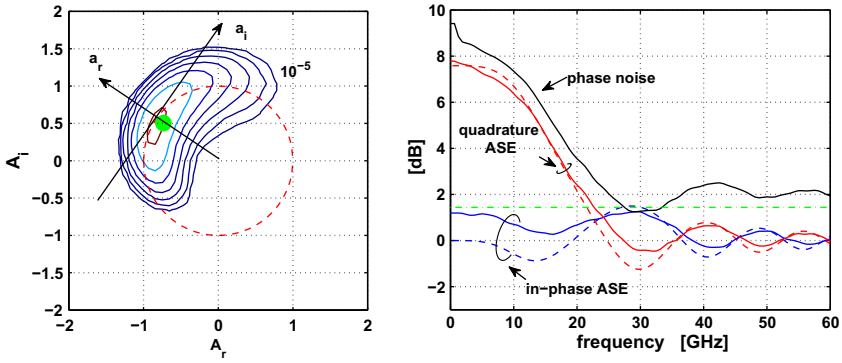

Fig. 3. (Left) Simulated probability density function (PDF) contours (down to 10^{-5}) of received field (CW + ASE) after a 20×100 km DM link with fiber dispersion $D_{tx} = 4$ ps/nm/km, zero in-line, −85 ps/nm pre-compensation, zero net residual dispersion, OSNR = 12 dB/0.1 nm and CW power 4.6 dBm,*after* optical filter of bandwidth 18 GHz. (Right) Solid lines: simulated power spectral density (PSD) of in-phase (S_{ar}) and quadrature (S_{ai}) ASE, and of the received field phase noise (S_ϕ) versus frequency *before* optical filter. Dashed lines: ASE PSD predicted with small-signal model in [16]. Dash-dotted horizontal line: field phase PSD in absence of PG.

Fig. 3(left) shows the contours of the PDF of the normalized received field $\tilde{A} = A_r + jA_i = e^{-j\Phi_{NL}}(1 + a_r + ja_i)$, where Φ_{NL} is the phase of the average value of $\tilde{A}$, which is much larger than 0.6π rad because of the significant total ASE power over the simulated bandwidth of ±80 GHz. The PDFs are taken *after* an optical receiver filter of bandwidth 18 GHz, and display the well-known "bean-like" non-elliptical contours down to probability 10^{-5} which make the received noise non-Gaussian and are the signature of single-channel NSNI. For the same 10^7 time-samples used to obtain Fig. 3(left), Fig. 3(right) shows the estimated PSDs S_{ar}, S_{ai} of the in-phase and quadrature ASE components, respectively (i.e., as shown in Fig. 3(left), the "radial" a_r and "tangent" a_i ASE components relative to the received CW), and the PSD S_ϕ of the phase of the received field (after subtraction of the average phase Φ_{NL}), all measured *before* the optical filter. The dash-dotted horizontal line is the PSD of S_ϕ in absence of nonlinear Kerr effects (no-PG), which is higher than the no-PG level of S_{ai} because $|\phi| > |\sin\phi| \simeq |a_i|$, as explained in detail in Appendix A. All PSDs are normalized to the no-PG common PSD level of a_r, a_i. Dashed lines also show the ASE PSD predictions of a linear model of PG in DM links [15,16], valid at large OSNR. The predicted theoretical normalized PSD values at $f = 0$ are

$$\begin{aligned} S_{ar}(0) &= 1 \\ S_{ai}(0) &= 1 + \frac{4}{3}\Phi_{CW}^2 \end{aligned} \tag{1}$$

i.e., 0 and 7.58 dB, respectively. The linear PG model postulates that the output ASE field is a linear filtering of the generated Gaussian ASE field, hence it retains Gaussian statistics, with elliptical PDF contours.

From Fig. 3 we note that:

(a) While the linear PG model incorrectly predicts Gaussian PDF contours of the field, its predictions of the PSD of the in-phase and quadrature ASE are quite good, except for an important under-estimation of the true in-phase PSD near zero frequency. Such an under-estimation, present only at large enough nonlinear phases, is connected to the bean-like bending of the field PDF observed in Fig. 3(left) which induces both a variance increase and a non-zero negative mean value of the radial a_r component, as seen from the average field (circle marker) sinking slightly inside the unit circle in Fig. 3(left).[1] Note that, since a significant PDF bending induces a marked increase of the zero-frequency PSD S_{ar}, the following simple formula ([17], Eq. (11)):

$$P_{th} = K\left(\sqrt{|\beta_2|}\mathrm{OSNR}\right)^{1/4} \tag{2}$$

valid for zero in-line dispersion maps, relates the CW power P_{th} that causes a given zero-frequency increase of S_{ar} to the OSNR and the transmission fiber dispersion β_2, through a system-dependent constant K. Hence this formula is also useful to predict at which power level one should expect significant PDF bending, and how it scales with OSNR and fiber dispersion.

(b) The spectral shape of the received phase can be reasonably inferred from that of the quadrature ASE, except for an offset in the "white" high-frequency level, that, as explained in the Appendix A, at lower OSNRs would be present even in absence of PG.
Fig. 4 shows the PSD of phase and ASE quadrature processes for increasing (left to right) OSNR, with the same data as in Fig. 3, except that signal power is lower ($P_{tx} = 1.6$ dBm). The figure clearly confirms that the spectral shape of the phase noise is always well predicted from the shape of the quadrature PSD.

(c) It was shown in [16] that the quadrature ASE PSD (and thus also the phase noise PSD) in DM links with small in-line dispersion displays a significant enhancement from the no-PG white level because of signal–noise interaction over a one-sided bandwidth of about

$$f_\Delta \triangleq \frac{1}{2\pi\sqrt{|\beta_2|/\alpha}} \tag{3}$$

with β_2 the transmission fiber dispersion and α the fiber attenuation. The parametric signal–noise interaction vanishes at frequencies above $2f_\Delta$. In our simulation, $f_\Delta \sim 16$ GHz, hence the optical filter of one-sided bandwidth $B_0 = 9$ GHz filters off not only the white high-frequency components, but also part of the colored, PG-inflated spectrum.
If we over-simplify the phase noise PSD with a rectangular approximation of the quadrature ASE PSD of constant level $S_{ai}(0)$ up to f_Δ and 1 otherwise, then we see from (1) that a very rough approximation of the phase noise variance can be obtained as

$$\mathrm{VAR}[\phi] = \int_0^{B_o} N_0 S_\phi(f)\mathrm{d}f \sim N_0\left(B_o + f_\Delta\frac{4}{3}\Phi_{CW}^2\right) \tag{4}$$

where N_0 is the quadrature ASE PSD level in absence of PG, and we assumed $f_\Delta < B_o$. The first term $N_0 B_o$ in (4) can be though of as the variance of the linear phase noise, i.e., the white phase noise generated by the white additive Gaussian ASE field in absence of PG. The second term $N_0 f_\Delta \frac{4}{3}\Phi_{CW}^2$ can instead be viewed

[1] Such a sinking occurs upstream of the optical filter, but when the optical filter has unit zero-frequency response, as in our case, the field average before and after the filter is the same.

Please cite this article in press as: A. Bononi et al., Nonlinear signal–noise interactions in dispersion-managed links with various modulation formats, Opt. Fiber Technol. (2009), doi:10.1016/j.yofte.2009.11.001

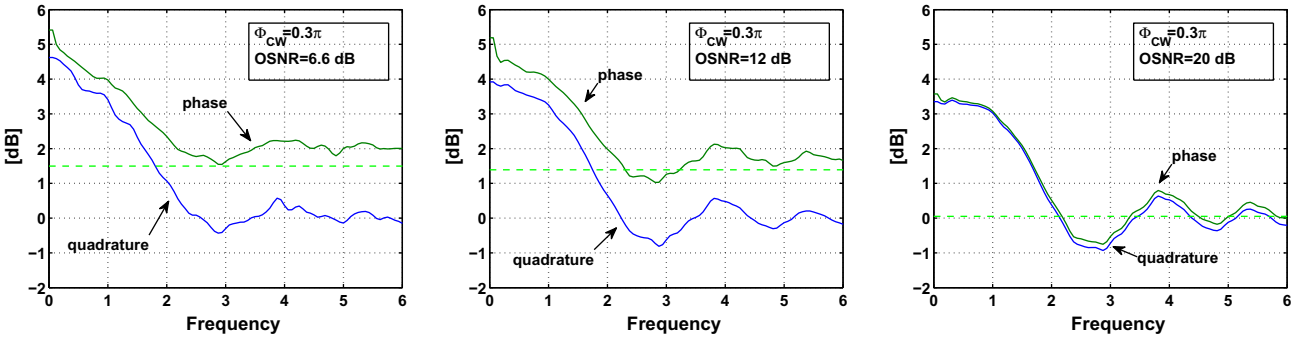

Fig. 4. Power spectral density of phase noise and ASE quadrature processes for increasing (left to right) OSNR [dB/0.1 nm]. Same data as in Fig. 3, except that signal power is halved ($P_{tx} = 1.6$ dBm, i.e., $\Phi_{CW} = 0.3\pi$). Dashed horizontal line: field phase PSD in absence of PG.

as the variance of the NLPN, i.e., the extra phase noise generated by the extra non-Gaussian non-white ASE field when PG is present. It is clear that, as we increase the baudrate and thus the optical filter bandwidth B_o, the variance of the linear phase noise will grow larger and larger, so that the NLPN will contribute a smaller and smaller fraction of the total phase noise variance. As this happens, also the total noise field, seen as a mix of white Gaussian "linear" ASE field and PG-correlated non-Gaussian non-linear ASE field, will tend to become more Gaussian.

From the features observed in Figs. 3 and 4, we can make the following system considerations:

(1) For intensity modulated signals such as OOK, it is the received field noise in the "radial" direction a_r, i.e., the amplitude noise, that mostly affects performance.
At large OSNR, when the linear PG model is applicable, one can even find maps which give amplitude noise squeezing and hence performance improvement. However, at large OSNR the observed PG-induced gain/penalty is generally negligible [17].
OOK single-channel propagation is instead most impacted by PG in the low-OSNR regime typical of FEC coded systems. It was shown in [17] that in this case OOK performance is markedly degraded by PG when the zero-frequency in-phase PSD level S_{ar} doubles with respect to its no-PG value (PG-doubling). The enhancement at zero frequency is due to the ASE–ASE beating during propagation. Hence the dominant single-channel NSNI manifestation in low-OSNR OOK propagation is an enhanced low-frequency nonlinear amplitude noise (NLAN) connected to the OOK field PDF bending.

(2) For phase-modulated signals, performance is instead set by the noise on the phase of the received field, i.e., the sum of a white linear phase noise, and of a colored NLPN [14] generated by the self-phase modulation (SPM) due to ASE-induced intensity fluctuations along the DM line. This is by far the dominant manifestation of the single-channel NSNI in phase-modulated systems. The system impact of NLPN eventually vanishes as the signal baudrate is increased, as clearly understood at the previous point (c).
The statistics of NLPN and their impact on phase-modulated systems were studied analytically in the past only at zero group velocity dispersion (GVD) [13,14,18,19]. In particular, the model by Ho [13,18] for the derivation of the NLPN PDF at zero GVD considers ASE propagation only on the signal's bandwidth, and thus neglects the effect of the receiver optical filter on the ASE field statistics and thus on NLPN statistics. In absence of the tight optical filtering around the carrier along the DM line assumed by Ho (i.e., in the usual case), and with negligible GVD, the ASE PSD gets colored over a huge frequency band; when the ASE gets finally filtered at the receiver, its statistics get back to Gaussian [20]. Ho's BER predictions for 10 Gbaud DPSK and DQPSK in DM lines with standard single mode fiber (SMF) are close to real because the effective bandwidth f_Δ over which the ASE quadrature PSD is enhanced above its linear white level is about 7 GHz, so that the nonlinearly-inflated ASE is actually present only over the signal's bandwidth, as in Ho's theory. This observation also hints to the fact that, for single-channel simulations with physically meaningful PG results, the SSFM fast-Fourier transform frequency window should encompass at least the $\pm 2f_\Delta$ range, i.e., the spectral range of significant NSNI in order to correctly reproduce the first-order FWM products between signal and noise. Note that we discussed NSNI models based on the CW signal assumption, because our subsequent numerical results will mostly refer to non-return to zero (NRZ) supporting pulses. However, for RZ shaped pulses, very refined perturbation theories have been established in the framework of DM solitons so that it is possible to evaluate the phase noise variance induced by ASE on soliton-like pulses [21,23–25].

2.2. WDM NSNI

Cross-phase modulation (XPM) is usually the dominant nonlinear effect in 10 Gb/s WDM OOK DM transmissions over non-zero dispersion fiber [6]. With OOK neighboring channels, the XPM is almost entirely due to the modulation-induced large intensity excursions of such channels, and ASE-induced intensity noise is a second-order effect. However, in WDM DQPSK and coherent QPSK homogeneous transmissions (i.e., where all channels have the same modulation format), all the neighboring channels have a periodic envelope, and thus the XPM induced by the periodic intensity fluctuations gets completely suppressed by the phase difference operation performed by the interferometric DQPSK receiver [26] or by the generalized phase difference operation [27] performed by the M-power phase estimation commonly implemented in DSP-based coherent receivers [8]. In such a case, what is left is the XPM due to non-periodic intensity fluctuations induced by ASE, which becomes a first-order impairment: we call this nonlinear effect as cross-NLPN (X-NLPN) [6]. It is a Gaussian process when XPM distortions can be modeled as small-signal perturbations. What in OOK is a second-order (and thus always neglected) effect, in phase-modulated systems emerges as a potentially dominant source of performance degradation [28].

3. System simulations

Purpose of this section is to perform a systematic study by simulation of the range of system parameters for which NSNI is the

Please cite this article in press as: A. Bononi et al., Nonlinear signal–noise interactions in dispersion-managed links with various modulation formats, Opt. Fiber Technol. (2009), doi:10.1016/j.yofte.2009.11.001

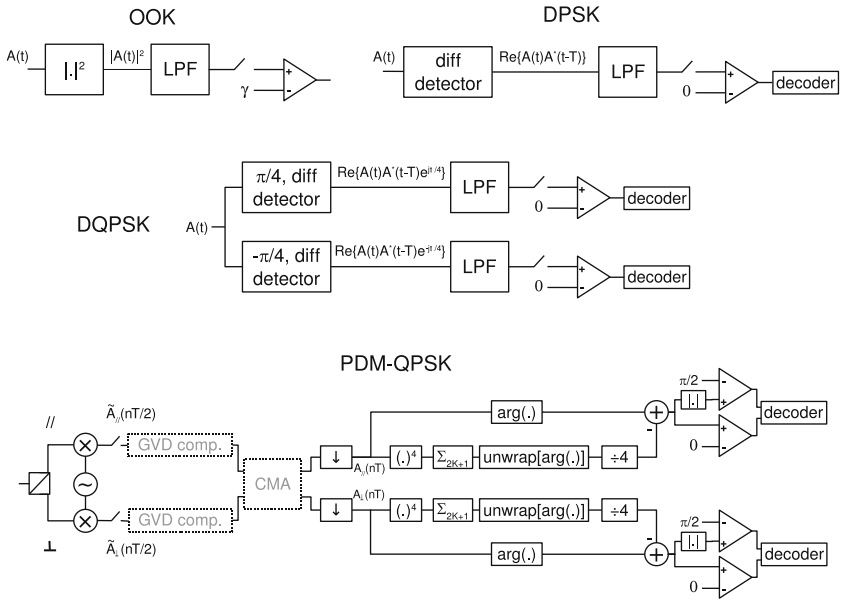

Fig. 5. Logical block diagrams of physical receivers in Fig. 1. For OOK: decision threshold is $\gamma > 0$. For D(Q)PSK threshold is zero. For PDM-QPSK: GVD compensation and CMA are actually not implemented in the simulations, since ideal linear optical channel inversion is assumed. This allows the analysis to concentrate on the action of the M-power phase estimation.

dominant nonlinear impairment for the analyzed modulation formats. The analytical models described in the previous section will ease our interpretation of the simulation results. We will also explore the role of other nonlinearities in comparison with NSNI.

We first introduce the simulation details, and then move to the results.

Let's start with the details of the various modulation formats. All simulations were performed with the open-source software *Optilux* [29], and the fine details of the simulation blocks can be found in the online documentation. All modulation formats were obtained (if not otherwise stated) from NRZ supporting electrical pulses, with raised-cosine shape with roll-off 0.2. Such pulses drove at different bias points a Mach–Zehnder modulator with DC extinction ratio $\epsilon = 13$ dB.

Fig. 5 shows the logical block diagrams with the operations performed in the simulation of the receiver physical structures of Fig. 1. All receivers were preceded by a Butterworth-6 optical filter with bandwidth 1.8 times the symbol rate R. The electrical low-pass filter (LPF) for OOK and D(Q)PSK was a Bessel-5 of bandwidth $0.65R$.

For the coherent receiver, we assumed the local oscillator had the same frequency as the incoming selected channel and no phase noise. GVD compensation was performed by a post-compensation fiber in the optical domain as for all other formats, hence the dashed "GVD comp." block was actually not implemented. Also, in the PDM-QPSK case the post-compensation fiber was also assumed to have a Jones matrix equal to the inverse of the Jones matrix of the DM line, so that ideal equalization of linear polarization distortions took place in the optical domain. Hence the dashed "CMA" block was actually not implemented. Such simplifications allow us to concentrate on the effect of the M-power phase estimator on performance. The M-power phase estimator forms the averaged M-power field process

$$E_i = \frac{1}{2K+1}\sum_{n=-K}^{K} A_{i-n}^4 \tag{5}$$

from the samples of the received phase-modulated noisy field A_n, where K will be called the *V&V tap parameter*, and provides the following estimated reference phase at the ith symbol time [30,12]:

$$\hat{\theta}_i = \frac{1}{4}\mathrm{unwrap}[\arg(E_i)] \tag{6}$$

where the unwrap operation is necessary to eliminate "equivocation" [31] due to crossing of the branch-cut of the complex plane by the averaged M-power field. Elimination of equivocation, unfortunately, triggers cycle-slips [30,32], a phenomenon that is only visible at low OSNR and makes the M-power phase estimator (6) biased.

In the coherent receiver we did not include any electronic nonlinear phase noise compensation [7,19] nor nonlinearity compensation by back-propagation [10].

Let's now move to describe the transmission line.

We considered again the 20×100 km terrestrial DM line sketched in Fig. 2. While in Section 2 a low-dispersion $D_{tx} = 4$ ps/nm/km and zero in-line dispersion were selected to show a system in which NSNI is emphasized, for the results in this section we selected a more common SMF transmission fiber (dispersion $D_{tx} = 17$ ps/nm/km, nonlinear coefficient $\gamma = 1.4\ \mathrm{W^{-1}km^{-1}}$), with a practical in-line RDPS $D_{in} = 30$ ps/nm. As in Section 2, pre-compensation was selected according to the single-channel noiseless-optimized *straight-line rule* (SLR) [2,33]:

$$D_{pre} = -\frac{D_{tx}}{\alpha} - \frac{N-1}{2}D_{in} \tag{7}$$

for OOK and

$$D_{pre} = -\ln(2)\frac{D_{tx}}{\alpha} - \frac{N-1}{2}D_{in} \tag{8}$$

for PSK modulations, amounting to -625 ps/nm for OOK and -521 ps/nm for phase modulations, respectively.

Single-channel noiseless-optimized net residual dispersion $D_{tot} = D_{pre} + ND_{in} + D_{post}$ was selected according to the rule [2]:

$$D_{tot} = \frac{\sqrt{2}}{8}\frac{\Phi}{1+\frac{4}{3\sqrt{3}}\Phi^2} \tag{9}$$

for OOK, with Φ the peak signal nonlinear phase, and $D_{tot} = 0$ for phase modulations.

All simulated fibers had zero dispersion slope, and compensating fibers were linear. For all formats excluding PDM-QPSK the propagation was scalar, corresponding to a worst-case with all

Please cite this article in press as: A. Bononi et al., Nonlinear signal–noise interactions in dispersion-managed links with various modulation formats, Opt. Fiber Technol. (2009), doi:10.1016/j.yofte.2009.11.001

channels aligned in polarization. For PDM-QPSK, the vectorial SSFM propagation in each fiber was implemented with the Manakov equation [34], PMD was zero, and the input states of polarization (SOP) of the WDM channels were random.

In WDM simulations, we assumed all channels had the same modulation format, and we fixed the fractional bandwidth utilization (FBU) $\eta \triangleq \frac{R}{\Delta f}$ to 0.4, where Δf is the channel spacing, so that, e.g., at $R = 40$ Gbaud, we had $\Delta f = 100$ GHz. We thus varied the spacing Δf when varying R, so that a fair performance comparison at different symbol rates could be made without incurring in excessive channel-overlap in the frequency domain.

We scaled the number of channels N_{ch} with the symbol rate according to the law [35]:

$$N_{ch} = \left\lceil \frac{\eta}{S} \right\rceil \tag{10}$$

where $S = \frac{|\beta_2|}{\alpha} R^2$ is the map strength and $\lceil . \rceil$ is the ceiling function. This criterion ensures that enough WDM channels are considered when XPM is dominant [35]. For instance, at $R = 10$ Gbaud and $D_{tx} = 17$ ps/nm/km, we used $N_{ch} = 11$, i.e., 5 channels on each side of our test central channel; at $R = 5$ Gbaud, we used $N_{ch} = 37$.

In WDM simulations, the number of discrete points per symbol, i.e., the inverse of the Nyquist frequency, was scaled as:

$$N_t = 2^{\left\lceil \log_2 \left(3 \frac{\Delta f (N_{ch}-1)}{R} \right) \right\rceil}$$

i.e., we forced it be a power of 2 and such that the entire fast-Fourier transform (FFT) spectrum covers at least three times the WDM bandwidth. Hence, our simulations capture at least first-order FWM. The maximum SSFM nonlinear phase per step was 0.003 rad. For the NRZ pulse shaping case, no optical filtering was applied at the transmitter, so that at $\eta = 0.4$ some spectral overlap, and thus linear crosstalk, was present.

Let's finally describe the BER evaluation process.

In deriving the results with NSNI we resorted to direct MC error counting. Theory was used mostly to interpret the simulation results. Some analytical models were used when NSNI was absent, i.e., when noise loading was used, as explained next.

For time efficiency, different simulation methods were used in the case of noise loading and in the case of distributed ASE generation, although in some circumstances (discussed below) the same method was used:

(i) In the noise loading case, BER was estimated from a single noiseless SSFM run with a De Brujin signal sequence of appropriate length that captures all relevant ISI patterns [2]. A single run was performed even in the WDM case, by assuming in-phase and time-aligned channels modulated with different De Brujin sequence seeds. WDM channels got time-decorrelated by the pre-compensating fiber; however, random channel timing has a very limited impact on performance of DM systems with in-line compensation [36]. Transmitter laser phase noise was ignored even in coherent simulations, since NLPN is largely dominant in the scenario under study.
After the noiseless SSFM propagation, for the OOK, DPSK and DQPSK format we used the KL pseudo-analytical method of BER evaluation [4] (which is much faster, although equivalent to MC error counting), while for the coherent receiver, white Gaussian optical ASE samples were loaded at the receiver and MC errors were counted.

(ii) In the distributed ASE case that captures NSNI, instead, BER was estimated by MC error counting for all formats (since the basic KL methods use white ASE. Although the KL method can be adapted to the PG case with non-white ASE [37], the BER results are only approximated, and for consistency with receivers simulated with the slower but "exact" MC method we decided to use MC for all formats). In each MC run the transmitted signal FFT window contained a block of 256 newly generated independent random symbols, as well as random ASE noise samples added at each amplifier. In all MC error counting simulations, the MC runs were stopped when the relative estimation error $\hat{\epsilon} = \frac{\hat{\sigma}_{BER}}{BER}$, i.e., the ratio of BER standard deviation and estimated BER, went below a given threshold, e.g., 0.1 or 0.05. Since $\hat{\epsilon} \sim \frac{1}{\sqrt{E[errors]}}$, that choice corresponded on average to counting either 100 or 400 errors [38].

To get an idea of how many SSFM propagation runs are necessary on average in the distributed ASE case, consider that on average one needs 10^5 symbol receptions to collect 100 symbol errors at a symbol error rate of 10^{-3}, i.e., $\frac{10^5}{256} \sim 400$ runs. Hence distributed ASE simulations require about 400 SSFM propagations at $\hat{\epsilon} = 0.1$, and 1600 propagations at $\hat{\epsilon} = 0.05$, as opposed to a single propagation (although with a longer FFT window) with noise loading.

Note that, even with noise loading, the use of shorter FFT windows with a reduced number of truly random symbols has been shown to be preferable over the use of long De Brujin sequences when the channel BER is large (e.g., BER $= 10^{-3}$) and at large map strength, when the memory of the DM line is large [39]. For instance, when the baudrate is 100 Gbaud, the memory of our SMF DM system is close to 17 symbol times [2], so that in the OOK case De Brujin sequences of 2^{17} should be employed, which is too time demanding: in this case it is faster to transmit many times a shorter sequence of random symbols, whose length exceeds the system memory.

3.1. Single-channel Q-penalty

Fig. 6 shows Q-factor in decibels, defined as $Q[\text{dB}] = 20\log_{10}[\sqrt{2}\text{erfc}^{-1}(2 \cdot \text{BER})]$, versus average transmitted power P_{tx} (top-left plot) for fixed OSNR for a 10 Gbaud OOK modulation, and Q-penalty with respect to back-to-back in the top-right plot, obtained from the same data as in the left plot. Dashed lines indicate noise loading, solid lines indicate distributed ASE. Similar plots were first obtained in [40], and are quite effective in showing the decrease in Q-factor due to the onset of nonlinear effects. The total dispersion D_{tot}, also plotted in Fig. 6(top-left), was chosen according to (9). The reason for the strange non-monotone behavior of the Q-factor can be attributed to the interplay between nonlinearly-induced ISI and PG.

In order to better understand such an interplay, Fig. 6(bottom-left) shows Q-factor versus total dispersion D_{tot} for two selected values of transmitted power $P_{tx} = [4.2, 1.2]$ dBm. At the noiseless optimum values $D_{tot} = [562, 777]$ ps/nm predicted by formula (9) we see that indeed the dashed "noise loading" curves reach their maximum: hence such values of D_{tot} maximally compress the pulses to minimize ISI. However, in the presence of PG the effect of the post-compensation fiber is that of mixing the in-phase and quadrature ASE components [16] by converting the nonlinear phase noise into intensity noise. We thus understand that, in absence of nonlinearly induced ISI, as for example in the "CW" curve in Fig. 6(bottom-right) where an all "1" sequence was transmitted, the optimal choice to reduce PG penalty in OOK is to completely remove the post-compensating fiber (i.e., use $D_{tot} = D_{pre} + ND_{in} = -50$ ps/nm). In presence of both modulation (i.e., ISI induced by SPM) and PG thus the optimal D_{tot} is somewhere between -50 and the noiseless optimal value (9).

The small humps in Q-factor with PG observed in Fig. 6(top-left) at P_{tx} between 5 and 6 dBm can be attributed to in-phase noise squeezing, which is particularly evident for positive dispersion transmission fiber when the in-line dispersion is positive [16].

Please cite this article in press as: A. Bononi et al., Nonlinear signal–noise interactions in dispersion-managed links with various modulation formats, Opt. Fiber Technol. (2009), doi:10.1016/j.yofte.2009.11.001

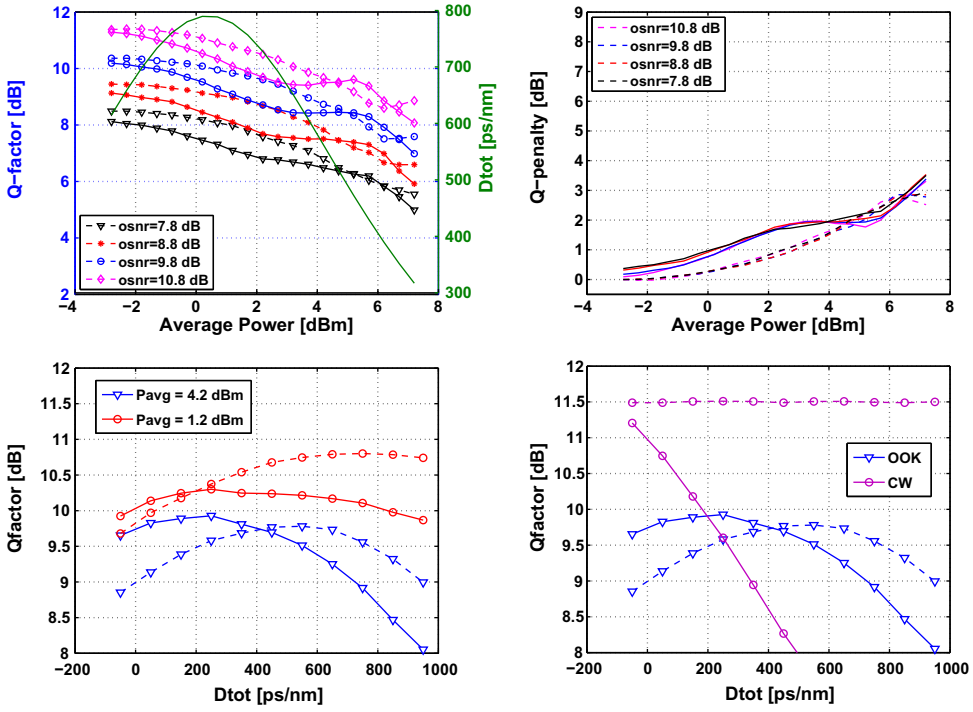

Fig. 6. (Top-left) Q-factor versus transmitted average signal power P_{tx} for $R = 10$ Gbaud NRZ-OOK for fixed *OSNR* in SMF 20×100 DM map with $D_{pre} = -650$ ps/nm, in-line 30 ps/nm/span and noiseless optimized D_{tot} (shown with parabolic shape, referred to right vertical axis); (top-right) Q-penalty versus P_{tx}. (Bottom-left) Q-factor versus total dispersion D_{tot} for two selected values of transmitted power $P_{tx} = 4.2$ dBm and $P_{tx} = 1.2$ dBm; (bottom-right) Q-factor versus D_{tot} at $P_{tx} = 4.2$ dBm for randomly modulated OOK (same as bottom-left), and for the 111... sequence (label CW). Dashed lines: noise loading. Solid lines: distributed ASE. MC relative error $\hat{\epsilon} = 0.05$ (i.e., 400 errors on average).

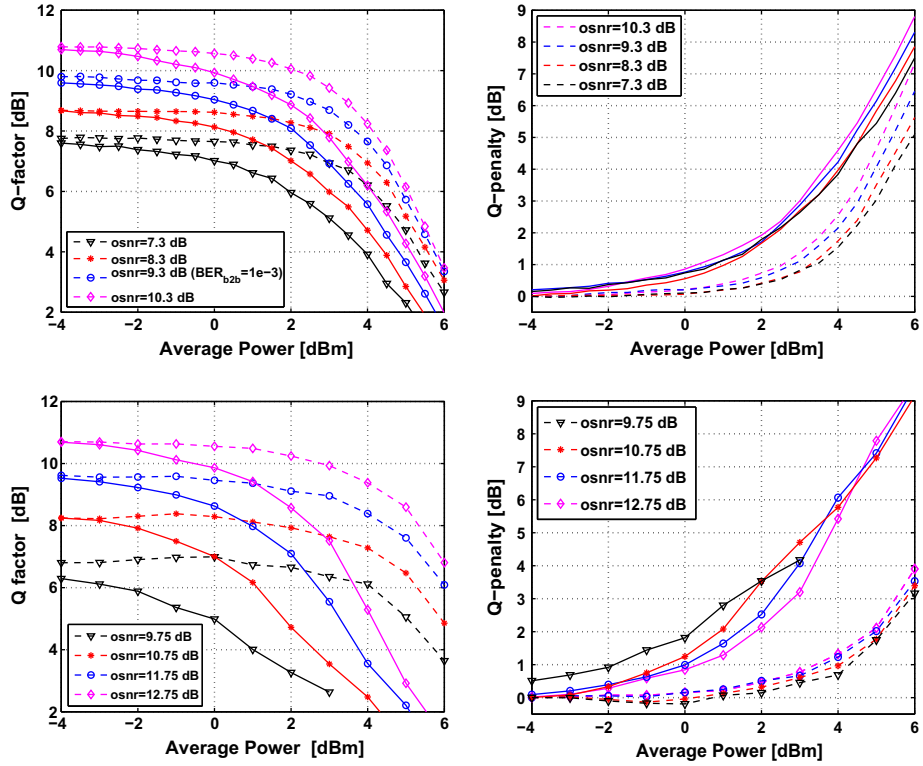

Fig. 7. (Left column) $20\log_{10}(Q\text{-factor})$ versus transmitted average signal power P_{tx} for fixed *OSNR* in SMF DM map with in-line 30 ps/nm/span; (right column) Q-penalty versus P_{tx}. (Top row) for 20 Gbaud NRZ-DQPSK; (Bottom row) 10 Gbaud NRZ PDM-QPSK with V&V tap parameter $K = 3$. Dashed lines: noise loading. Solid lines: distributed ASE. MC relative error $\hat{\epsilon} = 0.05$ (i.e., 400 errors on average).

Please cite this article in press as: A. Bononi et al., Nonlinear signal–noise interactions in dispersion-managed links with various modulation formats, Opt. Fiber Technol. (2009), doi:10.1016/j.yofte.2009.11.001

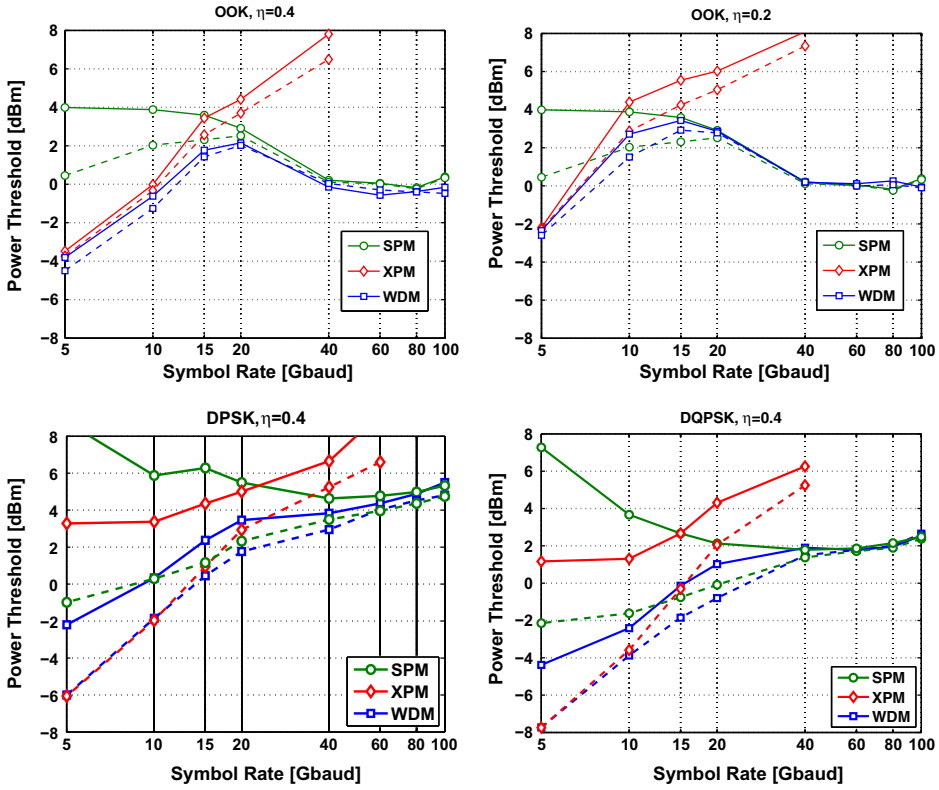

Fig. 8. Power threshold for SMF DM line for: (top-left) NRZ-OOK, $\eta = 0.4$ (top-right) NRZ-OOK $\eta = 0.2$, (bottom-left) NRZ-DPSK $\eta = 0.4$, (bottom-right) NRZ-DQPSK $\eta = 0.4$. All plots: Solid: noise loading; Dashed: distributed ASE; "SPM", single-channel; "XPM", (no SPM, no FWM); "WDM", all nonlinear effects. No TX filtering. MC relative BER estimation error $\dot{\epsilon} = 0.1$, i.e., 100 errors on average.

Let's now turn to phase-modulated formats. For the same 20×100 km SMF DM line as in Fig. 6, Fig. 7 shows the corresponding Q-factor (left column) and Q-penalty (right column) versus average P_{tx} for (top row) 20 Gbaud DQPSK and (bottom row) 10 Gbaud coherent PDM-QPSK, respectively. For phase modulations, the noiseless optimal D_{tot} is close to zero (in fact, slightly positive and increasing with P_{tx}). However, here post-compensation plays a minor role with PG, since the conversion of intensity to phase noise is irrelevant.

The major difference among the formats is that in the OOK case the Q-penalty due to NSNI is much smaller (at equal average power) than in the phase-modulated cases, where the Q-penalty monotonically and very rapidly increases with P_{tx}. The reason is that NSNI manifests itself mainly as nonlinear phase noise, with an "inflation" of the quadrature ASE PSD in all DM maps, while the in-phase (radial) ASE component is little affected by the map, until PDF bending sets in.

3.2. Nonlinear threshold

The previous results were restricted to single-channel propagation, and were obtained for specific choices of map strength. They were intended to highlight with some examples the interplay between SPM and PG in various modulation formats. To get a more global view of the DM design in presence of NSNI, we next present the transmitted average power (called *nonlinear threshold*, NLT) that gives 1 dB of OSNR penalty at BER $= 10^{-3}$ [41], and show how it changes as the symbol rate increases, both for a single-channel and for a WDM homogeneous system. The reference DM line will again be the 20×100 km SMF terrestrial system of the previous section with 30 ps/nm RDPS.

Our target in this section is to understand the dominant nonlinear effects as the baudrate R (in fact, as the map strength S) increases.

The procedure for the measurement of the NLT is detailed in Algorithm 1.

Algorithm 1. *NLT measurement algorithm.*

1. Measure the OSNR [dB/0.1 nm] in back-to-back (b2b) that gives BER $= 10^{-3}$. E.g. for $R = 10$ Gbaud we got $OSNR_{10} = [6.6, 9.3, 8.75, 11.75]$[dB/0.1nm] for DPSK, DQPSK, single polarization QPSK and PDM-QPSK, respectively. The OSNR in b2b scales with the symbol rate R as $OSNR_R = OSNR_{10} + 10\log_{10}(R/10)$.
2. Since the threshold is at 1 dB of OSNR penalty, we search it by setting the OSNR to $OSNR = OSNR_R + 1$dB.
3. Fix a tentative transmitted power P_{tx}. The noise figure (NF) of the amplifiers of the DM line is obtained from the ASE power $N_A = OSNR/P_{tx}$. Signal is SSFM propagated and BER is measured in such a DM line. If BER $< 10^{-3}$ (BER $> 10^{-3}$) we increase (decrease) P_{tx} and repeat point 3.
4. The NLT is found by interpolation of the BER versus P_{tx} for the few tested points around 10^{-3}.

Each subplot in Figs. 8 and 9 shows, for a specific modulation format, the NLT versus symbol rate R for: (1) single-channel transmission (label "SPM"); (2) WDM transmission with solution of individual coupled NLSEs for all channels, with both self-phase modulation and FWM switched OFF (label "XPM"); such an intermediate result helps appreciate the contribution of the sole XPM to the NLT; (3) WDM comb propagated as a single-channel, hence with all nonlinearities ON (label "WDM"). In all three cases, we provide both the NLT obtained by noiseless signal SSFM propagation and receiver noise loading (solid lines) where NSNI is overlooked, and by noisy signal propagation with distributed ASE generation at each amplifier to include NSNI (dashed lines). Subplots in Fig. 8 refer to the following

Please cite this article in press as: A. Bononi et al., Nonlinear signal–noise interactions in dispersion-managed links with various modulation formats, Opt. Fiber Technol. (2009), doi:10.1016/j.yofte.2009.11.001

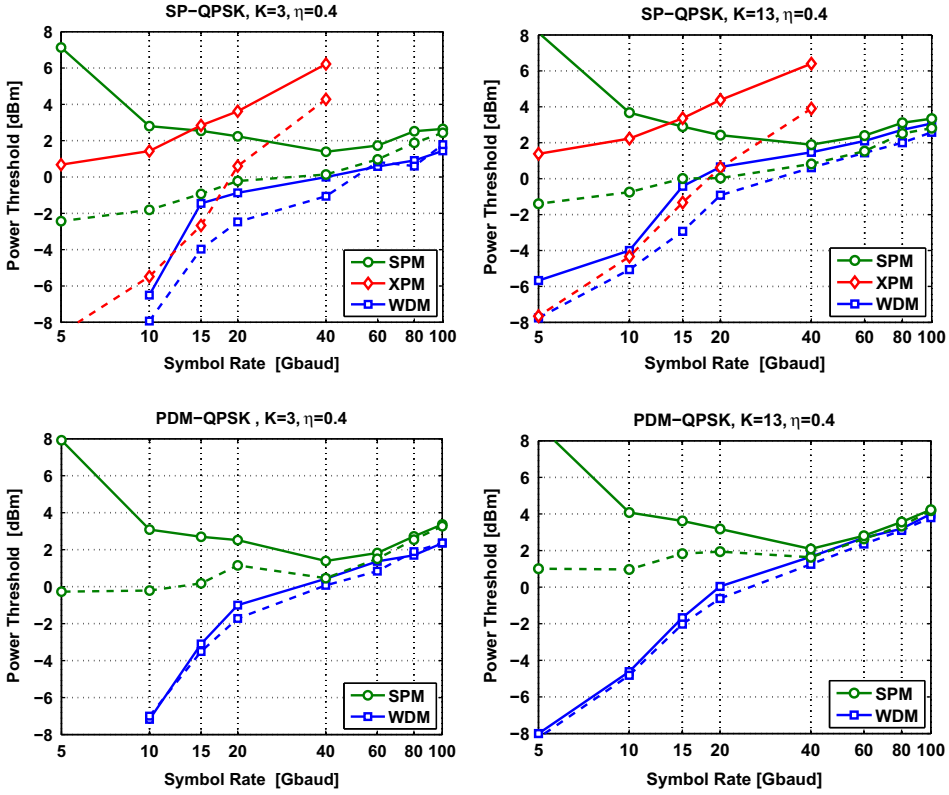

Fig. 9. Power threshold for SMF DM line for: (top-left) single polarization coherent NRZ-QPSK with V&V tap parameter $K = 3$, (top-right) single polarization coherent NRZ-QPSK with $K = 13$, (bottom-left) coherent PDM-NRZ-QPSK with $K = 3$, (bottom-right) coherent PDM-NRZ-QPSK with $K = 13$. All plots: Solid: noise loading; dashed: distributed ASE; "SPM", single-channel; "XPM", (no SPM, no FWM); "WDM", all nonlinear effects. Fractional bandwidth utilization $\eta = 0.4$. No TX filtering. Random input SOPs in PDM case. MC relative BER estimation error $\hat{\epsilon} = 0.1$, i.e., 100 errors on average.

modulation formats: (top-left) NRZ-OOK with $\eta = 0.4$; (top-right) NRZ-OOK $\eta = 0.2$; (bottom-left) NRZ-DPSK $\eta = 0.4$; (bottom-right) NRZ-DQPSK $\eta = 0.4$. In Fig. 9 we have ($\eta = 0.4$ in all plots):

(Top-left) coherent single polarization (SP)-NRZ-QPSK with V&V tap parameter $K = 3$; (top-right) coherent SP-NRZ-QPSK with $K = 13$; (bottom-left) coherent PDM-NRZ-QPSK with $K = 3$; (bottom-right) coherent PDM-NRZ-QPSK with $K = 13$.

The SP-QPSK case was simulated by scalar propagation and processing of only the X polarization, with all WDM channels aligned on that polarization. In this case, we also propagated only the X component of the ASE noise.

BER values leading to results in Figs. 8 and 9 were always estimated with a relative error $\hat{\epsilon} = 0.1$, i.e., 100 errors were counted on average.

To give a rough idea of the overall computational effort, reobtaining the data reported in Figs. 8 and 9 (with all the software tested, debugged and ready to run) would take over one month of processing time on a fully-dedicated 8-core processor. The slowest computations are those at the lowest symbol rates, where a large number of WDM channels is included for proper XPM rendering.

4. Discussion

(i) *OOK*

In the single-channel NRZ-OOK case, Fig. 8(top row), we note that NSNI (showing up here as NLAN), is significant at lower symbol rates, and ceases to be a problem at about 20 Gbaud in this SMF DM system. The x-axis should more properly be read as the strength $S \propto |D_{tx}|R^2$ [35], so that, e.g., for a fiber with $D_{tx} = 4$ ps/nm/km we expect NSNI to become negligible at 40 Gb/s. In the OOK WDM case with $\eta = 0.4$, Fig. 8 top-left, we note that noiseless XPM ("XPM" solid) is quite close to noisy XPM ("XPM" dotted), confirming that ASE on pumps is a second-order effect in XPM. From the closeness of the "XPM" solid line to the "WDM" dotted line, we can conclude that at lower baudrates noiseless XPM is the dominant nonlinearity in OOK. We see that the dotted "SPM" NLT is below the solid "XPM" NLT for baudrates $\gtrsim 15$ Gbaud, indicating that single-channel NLAN is the dominant nonlinearity. Such a dominance ceases at 20 Gbaud, where the "SPM" dotted and solid lines merge: at larger baudrates noiseless SPM (i.e., SPM induced single-pulse distortion and ISI) is the dominant nonlinearity. Over the entire baudrate range at $\eta = 0.4$ NSNI changes the NLT by less than 0.5 dB. Intuitively, we expect that moving to lower bandwidth utilization η will make the dominance of single-channel NSNI emerge more clearly, since the XPM NLT will markedly increase while single-channel NLT will stay the same. This is confirmed by Fig. 8 top-right, which reports the case $\eta = 0.2$. Here we observe that OOK is more significantly affected by NSNI, with a worst-case decrease of NLT from the noise-loading predictions by 1.5 dB at 10 Gbaud. Interestingly, note from the increased difference from the solid and dotted "XPM" curves that at $\eta = 0.2$ ASE on pumps ceases to be a truly second-order effect. Note also that at very large R the "SPM" and "WDM" curves with $\eta = 0.4$ do not match exactly since the single-channel simulation does not have the linear crosstalk added at the transmitter in the WDM case. The $\eta = 0.2$ curves do instead completely overlap since WDM linear crosstalk is negligible.

(ii) *D(Q)PSK*

A completely different behavior is observed with phase-modulated formats. In single-channel NRZ-DPSK and NRZ-DQPSK, Fig. 8(bottom row), we see that NSNI (showing up here as NLPN) imposes noticeably lower thresholds than in OOK. NSNI vanishes, i.e., solid and dashed "SPM" lines merge, at around 40 Gbaud in DQPSK, while in DPSK NSNI is still present even beyond 100 Gbaud. The vanishing of NSNI is connected to the fact that the signal–noise

Please cite this article in press as: A. Bononi et al., Nonlinear signal–noise interactions in dispersion-managed links with various modulation formats, Opt. Fiber Technol. (2009), doi:10.1016/j.yofte.2009.11.001

PG interaction bandwidth is a small fraction of the optical filter bandwidth, so that most of the ASE is white as in linear transmission, and thus the linear component of phase noise passed by the optical filter dominates over NLPN, as discussed at point (c) in Section 2. However, in DPSK the noiseless SPM NLT ("SPM" solid) is ~ 3 dB larger than in DQPSK, so that the relative importance of NLPN is larger, as seen from (4). Both for NRZ-DPSK and NRZ-DQPSK we note that the NLT is much larger than in NRZ-OOK at the largest baudrates.

In the WDM case, for DQPSK we see from the spread of solid and dashed "WDM" curves that NSNI must be taken into account at low symbol rates, while after ~ 40 Gbaud single-channel effects dominate and NSNI becomes negligible. As already observed from single-channel, in DPSK the merger of the solid and dotted "WDM" curves occurs at much larger R. Both in DPSK and DQPSK, comparison of "WDM" and "XPM" curves reveals that, while signal-induced XPM is negligible compared with the dominant nonlinearity in absence of NSNI ("XPM" versus "WDM" solid), the X-NLPN due to distributed ASE ("XPM" dashed) is the dominant WDM nonlinear impairment at low R. Above $R \sim 18$ Gbaud for DPSK and $R \sim 15$ Gbaud for DQPSK we see that single-channel NLPN ("SPM" dotted) dominates over XPM-NLPN ("XPM" dotted) up to 40 Gbaud where noiseless SPM takes over the role of dominant nonlinearity.

(iii) *Single-polarization coherent QPSK*

We will first discuss the single-polarization coherent QPSK, which can be immediately compared with incoherent DQPSK since it does not have the complications of vectorial propagation and polarization demultiplexing, and next move to the PDM-QPSK. The NLT versus R for SP-QPSK is shown in the top-left plot of Fig. 9 when using a V&V tap parameter $K = 3$. While in the single-channel case the performance ("SPM" curves) is similar to DQPSK, with a vanishing of NSNI at around 40 Gbaud, and in the WDM case we observe a vanishing of NSNI between 40 and 60 Gbaud as in DQPSK, the low-baudrate behavior is quite different: coherent QPSK has a very strong decrease of the NLT at lower R. Also the difference between "SPM" and "WDM" curves at $R > 60$ Gbaud is unexpectedly large: in this regime, single-channel effects dominate, and the only difference between "WDM" and "SPM" is the linear crosstalk due to spectral overlap being absent in the "SPM" curves. So why is that difference so larger than in DQPSK? The top-right plot in Fig. 8 shows the SP-QPSK case with a larger $K = 13$, and we see that most of the anomalies have disappeared and now the NLTs in SP-QPSK do resemble those in DQPSK.

The explanation of such a widely different behavior from WDM DQPSK can be traced back to the low-SNR behavior of the M-power phase estimator with low tap parameter K, and in particular to problems connected with the unwrap function. We provide here a brief explanation. In the NLT plots, the OSNR was scaled linearly with R and the optical filter bandwidth also scaled linearly with R, so that the electrical SNR ρ is the same for all values of R. Since we are studying the NLT at BER $= 10^{-3}$ the SNR is rather low, and the fourth power operation largely enhances the noise on the average field (5) [32], so that crossings of the branch-cut of the complex plane occur very frequently and not always the unwrap operation in (6) yields the correct phase trajectory. The appearance of phase-unwrap problems, and consequent cycle-slips, is visible only below a given SNR threshold ρ_{th}. Such a threshold decreases in presence of nonlinear phase noise, such as that triggered by the intensity variations due to spectral overlap from neighboring WDM channels, which is the reason of the dramatic decrease of the NLT in SP-QPSK with $K = 3$. However, the threshold ρ_{th} increases for larger values of the V&V tap parameter K, which explains the improvement in NLT with $K = 13$. A larger value of K has also the beneficial effect of reducing the impact of linear crosstalk at large baudrates, as seen by the reduced gap between "WDM" and "SPM" at large R.

(iv) *Coherent PDM-QPSK*

Finally, for PDM-QPSK (for which the "XPM" curves were not theoretically available[2]), we note in Fig. 9(bottom-left) that, while in the single-channel case NLPN is the dominant impairment up to 60 Gbaud, in the WDM case with $K = 3$ the impact of NSNI seems rather weak, with only 0.5 dB of NLT decrease with respect to noise loading in the range $20 < R < 60$ Gbaud. This is attributed to the dominant role of another WDM nonlinearity, namely cross-polarization modulation (XPolM), whose basic mechanisms can be explained by some existing analytical models developed for OOK [42–44] and have recently been quantified in terms of depolarization induced on a probe channel in a large WDM multiplex [45]. Recent observations have pointed out that correct reproduction of XPolM effects requires more WDM channels than those needed for XPM reproduction [46,45]. Hence our NLT results obtained with the XPM-based scaling (10) of the number of WDM channels may be optimistic in this respect. Fig. 9 (bottom-right) shows that increasing the V&V tap number to $K = 13$ has even in the PDM case a beneficial effect, with the disappearance of the NLT drop at lower baudrates. The NSNI impact, however, remains confined between 20 and 60 Gbaud and is smaller than 0.5 dB.

We conclude with some remarks on possible extensions of this work.

(1) All the previous simulations were performed with NRZ supporting pulses. How would NLT results change with RZ pulses?

It is known that with suitably short RZ pulses, and with particular DM maps, the NLPN can be reduced [22,23]. To test under which DM map conditions this is true, for the DQPSK format we performed again NLT simulations when choosing RZ pulses with a 33% duty cycle. Since channels at $\eta = 0.4$ are tightly packed, in this case we performed channel filtering at the transmitter with a super-Gaussian optical filter of order 3 and bandwidth $1.1R$ before wavelength multiplexing. The DM line and the receiver were the same as before. In this case the OSNR for BER $= 10^{-3}$ was 9.3 [dB/0.1 nm] at $R = 10$ Gbaud. Fig. 10(left) shows the NLT versus R for this format, and Fig. 10(right) shows the transmitted RZ and NRZ waveform intensities. The NLT should be compared with the NRZ-DQPSK NLT in Fig. 8(2nd row-left plot). We see that in the single-channel case at $R < 20$ Gbaud the RZ NLT is lower than that of NRZ shaping, mainly because the PG-inflated ASE PSD depend on an effective CW power P_{eff} that coincides with the peak RZ pulse power at low strengths [37]. For $R \gtrsim 20$ Gbaud instead the RZ shaping is effective in increasing the NLT, since P_{eff} tends to converge to the average signal power at larger strengths [37]. In the WDM case we note that the single channel ("SPM") and multi-channel ("WDM") curves merge at much smaller R with respect to the NRZ-QPSK case, both with noise loading (solid) and with NSNI (dashed). RZ-33 pulse shaping seems thus the right choice at 20 Gbaud, while at 10 Gbaud the NRZ shaping provides better performance.

(2) In this study, 30 ps/nm RDPS was used throughout. How would the impact of NSNI change with a different in-line RDPS? A thorough answer would imply repeating the extremely time consuming NLT simulations for a whole set of RDPS values, and this is clearly beyond the scope of this paper. Some theoretical considerations can however be made. Changes in the PG-induced ASE PSDs can be easily checked with the linear PG model [16], and maps with a reduced NLPN variance are easily found, e.g., by increasing the in-line RDPS. The trouble is that, while both NLPN and X-NLPN are reduced by a larger RDPS, usually ISI (i.e., "SPM") is largely increased, so that a trade-off is at work and the optimal RDPS will depend on the modulation format.

[2] Although coupled vectorial propagation equations for the WDM channels are known [44], it is unclear how to distinguish between XPolM and XPM operators in the vectorial case, in order to be able to switch XPolM OFF.

Please cite this article in press as: A. Bononi et al., Nonlinear signal–noise interactions in dispersion-managed links with various modulation formats, Opt. Fiber Technol. (2009), doi:10.1016/j.yofte.2009.11.001

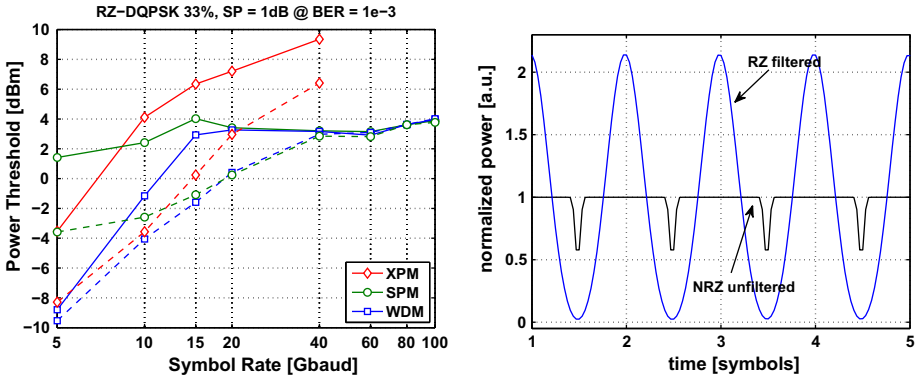

Fig. 10. (Left) NLT versus R for RZ-DQPSK with 33% duty cycle, MC estimation error. (Right) Transmitted field intensity in both NRZ and RZ. Filtering at transmitter with super-Gaussian-3 optical filter of bandwidth $1.1R$. Relative BER estimation error $\hat{\epsilon} = 0.1$.

(3) For coherent systems, no-DM maps where in-line compensation is avoided altogether are becoming a popular choice since cross-channel nonlinearities are strongly reduced. How important is here NSNI? Classical no-DM PG analysis [1,16] predicts that PG will vanish at frequencies beyond $\sqrt{2}f_c = \frac{1}{\pi}\sqrt{\frac{1}{|\beta_2|L_{NL}}}$, with L_{NL} the nonlinear length, while in DM links it will vanish beyond $2f_\Delta = \frac{1}{\pi}\sqrt{\frac{1}{|\beta_2|\alpha}}$. Hence the PG bandwidth reduction factor of no-DM with respect to DM with small in-line dispersion (at equal transmission fiber dispersion value) is $\sqrt{\frac{1/\alpha}{L_{NL}}}$. Therefore, in no-DM coherent systems the baudrate beyond which NSNI vanishes is expected to be largely reduced by such a factor. For instance, assuming a value $L_{NL} = 1000$ km, we expect such a baudrate for SP-(D)QPSK to decrease from 40 Gbaud in DM to 5 Gbaud in no-DM. However, as we have seen, only WDM SP coherent/incoherent phase-modulated systems are noticeably affected by NSNI.

(4) PMD was neglected in this study. How does PMD affect NSNI? It was reported in [47] that in coherent systems with electronic equalization of linear impairments, PMD has a beneficial effect in reducing NLPN, since intuitively ASE noise spikes are split and delayed on the two polarization axes, thus reducing their intensity to phase conversion operated by SPM.

(5) A final interesting question is whether distributed amplification, obtained for instance by forward–backward Raman pumping, is able to reduce the impact of NSNI. Intuitively, distributed amplification allows minimizing the needed signal power for a given target BER, hence reducing all nonlinearities, including NSNI, and experimental investigations confirm such a trend [48]. However, if this gain in performance could be seen as only due to a reduced noise figure of the line amplifiers, then the nonlinear threshold, as defined in this paper, would not be affected. Hence the only impact on NLT due to distributed amplification is connected with a change of shape of the nonlinear kernel in the distributed amplification case [16]. In the ideal case of perfect distributed compensation, i.e., a loss-less fiber, the 3-dB bandwidth of such a kernel is $f'_\Delta \sim \frac{1}{2\pi}\sqrt{\frac{3}{|\beta_2|z_A}}$ with z_A the span length [16], and this should be compared with the 3-dB kernel bandwidth in a lossy fiber given in Eq. (3): for e.g., $z_A = 100$ km the PG bandwidth is decreased only by a factor ~ 1.3 with respect to the lossy case. Hence we expect only a minor impact of distributed amplification on NLT. Moreover, in a practical Raman implementation of distributed amplification, other noise sources such as double Rayleigh back-scattering and pump-signal intensity-noise transfer are introduced, whose impact must be carefully traded against nonlinearity reduction.

5. Conclusions

In this paper we investigated by simulation the resilience of OOK, incoherent D(Q)PSK, and DSP-based coherent PDM-QPSK to nonlinear signal–noise interactions, and studied the nonlinear threshold behavior in optimized single-period terrestrial DM links for increasing map strength. The NLT analysis revealed the dominant nonlinear effects in the various transmission regimes. Fig. 11 shows a graphical qualitative summary of the dominant nonlinearity in WDM DM homogeneous systems as the strength of the map (i.e., the product $|D_{tx}|R^2$) increases. While in all formats at very low strength FWM is the dominant impairment [6], as the map strength increases we have that:

(1) For OOK the dominant nonlinearity is next noiseless XPM, then NLAN, and finally noiseless SPM;
(2) For single-polarization phase-modulated formats the dominant nonlinearity is next X-NLPN, then NLPN, and finally noiseless SPM;
(3) For PDM phase modulation the dominant nonlinearity is next XPolM, then NLPN, and finally noiseless SPM.

The ranges of dominance vary according to the channel spacing. From the quantitative analysis, we can conclude that in a WDM scenario over an SMF-based DM line at a large fractional bandwidth utilization $\eta = \frac{R}{\Delta f} = 0.4$ the trick of noise loading can be safely used in the simulation of both the OOK format and the PDM-QPSK format, while the DQPSK and coherent SP-QPSK formats are dominated by NSNI, except at baudrates larger than $R \sim 40$–60 Gbaud. At lower values of η even in the OOK case NSNI should be included in the simulations, but only in the restricted range $R \in [10, 20]$ Gbaud. An important finding for homogeneous

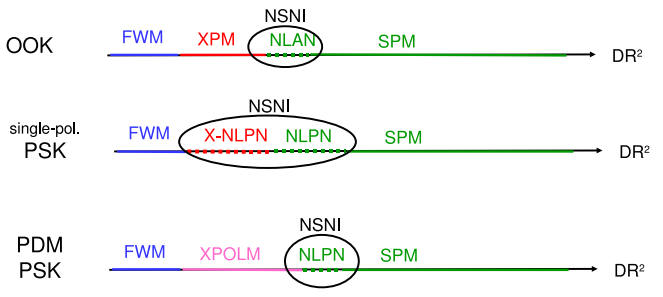

Fig. 11. Taxonomy of dominant nonlinearity in dispersion-managed homogeneous WDM systems.

Please cite this article in press as: A. Bononi et al., Nonlinear signal–noise interactions in dispersion-managed links with various modulation formats, Opt. Fiber Technol. (2009), doi:10.1016/j.yofte.2009.11.001

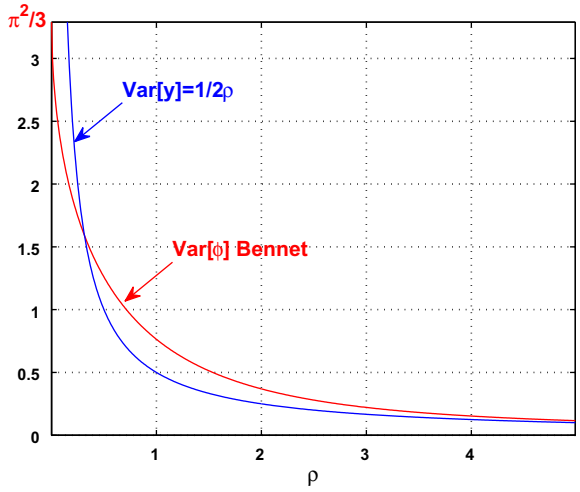

Fig. 12. Variance of Bennet phase and of quadrature noise.

WDM systems with coherent QPSK format is that in the M-power phase estimation the number of smoothing taps $2K+1$ should be large enough to avoid phase unwrapping problems when working near the NLT at BER $= 10^{-3}$. However, in hybrid systems with legacy 10 Gbaud OOK channels and higher-rate PDM-QPSK coherent channels, care must be taken with the choice of K: if the working OSNR is sufficiently large that no unwrap problems are present, then whenever XPM or any other low-frequency phase noise is dominant, a reduced K must be chosen [27] or, better yet, a smarter smoothing filter shape should be selected in the M-power phase estimation [32].

Acknowledgments

The authors acknowledge valuable feedback from S. Bigo, G. Charlet, E. Greiller, M. Salsi and G. Bellotti of Alcatel-Lucent.

Appendix A

Consider a real signal field of value 1 with complex additive circular Gaussian noise $a = a_r + ja_i$ of variance σ^2 per component. The phase of the total field ϕ has a Bennet distribution [49], whose variance is reported in Fig. 12 versus the signal-to-noise ratio (SNR) $\rho = \frac{1}{2\sigma^2}$. Also the variance of the quadrature noise component $\sigma^2 = \frac{1}{2\rho}$ is reported in the plot. At large SNR the variances coincide because ϕ coincides with a_i, but at smaller SNR the phase has larger variance. If the Gaussian noise comes from a white Gaussian process, then both a_i and ϕ are white processes over the receiver bandwidth B_o, with flat PSD S_{a_i} and S_ϕ, respectively. Since $Var[\phi] = S_\phi B_o$ and $Var[a_i] = S_{a_i} B_o$, from the above we conclude that $S_\phi > S_{a_i}$. Note that this relation ceases to be true at impractically low SNR, since the Bennet distribution tends to the uniform distribution over $[-\pi, \pi]$ with variance $\pi^2/3$.

References

[1] G.P. Agrawal, Nonlinear Fiber Optics, Academic, San Diego, 1995.
[2] A. Bononi, P. Serena, A. Orlandini, A unified design framework for single-channel dispersion-managed terrestrial systems, J. Lightw. Technol. 26 (2008) 3617.
[3] L.K. Wickham, R.-J. Essiambre, A.H. Gnauck, P.J. Winzer, A.R. Chraplyvy, Bit pattern dependence of intrachannel nonlinearities in pseudolinear transmission, Photon. Technol. Lett. 16 (2004) 1591.
[4] E. Forestieri, M. Secondini, On the error probability evaluation in lightwave systems with optical amplification, J. Lightw. Technol. 27 (2009) 706.
[5] A. Bononi, P. Serena, N. Rossi, Modeling of signal–noise interactions in nonlinear fiber transmission with different modulation formats, in: Proc. ECOC '09, paper 10.4.6.
[6] P.J. Winzer, R.-J. Essiambre, Advanced modulation formats for high-capacity optical transport networks, J. Lightw. Technol. 24 (2006) 4711.
[7] E. Ip, A.P.T. Lau, D.J.F. Barros, J.M. Kahn, Coherent detection in optical fiber systems, Opt. Exp. 16 (2008) 753.
[8] D.-S. Ly-Gagnon, S. Tsukamoto, K. Katoh, K. Kikuchi, Coherent detection of optical quadrature phase-shift keying signals with carrier phase estimation, J. Lightw. Technol. 24 (2006) 12.
[9] G. Charlet, Coherent detection associated with digital signal processing for fiber optics communications, C. R. Physique 9 (2008) 1012.
[10] G. Li, Recent advances in coherent optical communication, Adv. Opt. Photon. 1 (2009) 279.
[11] A.J. Viterbi, A.M. Viterbi, Nonlinear estimation of PSK-modulated carrier phase with application to burst digital transmission, Trans. Inf. Theory 29 (1983) 543.
[12] L.G. Kazovsky, G. Kalogerakis, W.-T. Shaw, Homodyne phase shift keying systems: past challenges and future opportunities, J. Lightw. Technol. 24 (2006) 4876.
[13] K.-P. Ho, Phase-Modulated Optical Communication Systems, Springer, New York, 2005.
[14] J.P. Gordon, L.F. Mollenauer, Phase noise in photonic communications systems using linear amplifiers, Opt. Lett. 15 (1990) 1351.
[15] A. Carena, V. Curri, R. Gaudino, P. Poggiolini, S. Benedetto, New analytical results on fiber parametric gain and its effects on ASE noise, Photon. Technol. Lett. 9 (1997) 535.
[16] P. Serena, A. Bononi, A. Orlandini, Fundamental laws of parametric gain in periodic dispersion-managed optical links, J. Opt. Soc. Am. B 24 (2007) 773.
[17] P. Serena, A. Bononi, J.-C. Antona, S. Bigo, Parametric gain in the strongly nonlinear regime and its impact on 10-Gb/s NRZ systems with forward-error correction, J. Lightw. Technol. 23 (2005) 2352.
[18] K.-P. Ho, Probability density of nonlinear phase noise, J. Opt. Soc. Am. B 20 (2003) 1875.
[19] A.P.T. Lau, J.M. Kahn, Signal design and detection in presence of nonlinear phase noise, J. Lightw. Technol. 25 (2007) 3008.
[20] A. Orlandini, P. Serena, A. Bononi, An alternative analysis of nonlinear phase noise impact on DPSK systems, in: Proc. ECOC'06, paper Th3.2.6.
[21] C.J. McKinstrie, C. Xie, T.I. Lakoba, Efficient modeling of phase jitter in dispersion managed soliton systems, Opt. Lett. 27 (2002) 1887.
[22] T. Mizuochi, K. Ishida, T. Kobayashi, J. Abe, K. Kinjo, K. Motoshima, K. Kasahara, A comparative study of DPSK and OOK WDM transmission over transoceanic distances and their performance degradations due to nonlinear phase noise, J. Lightw. Technol. 21 (2003) 1933.
[23] A. Tonello, S. Wabnitz, O. Boyraz, Duty-ratio control of nonlinear phase noise in dispersion-managed WDM transmissions using RZ-DPSK modulation at 10 Gb/s, J. Lightw. Technol. 24 (2006) 3719–3726.
[24] S. Kumar, Effect of dispersion on nonlinear phase noise in optical transmission systems, Opt. Lett. 30 (2005) 3278.
[25] S. Kumar, Analysis of nonlinear phase noise in coherent fiber-optic systems based on phase shift keying, J. Lightw. Technol. 27 (2009) 4722.
[26] K.-P. Ho, Error probability of DPSK signals with cross-phase modulation induced nonlinear phase noise, J. Sel. Top. Quantum Electron. 10 (2004) 421.
[27] A. Bononi et al., Cross-phase modulation induced by OOK channels on higher-rate DQPSK and coherent QPSK channels, J. Lightw. Technol. 27 (2009) 3974.
[28] H. Kim, Cross-phase-modulation-induced nonlinear phase noise in WDM direct-detection DPSK systems, J. Lightw. Technol. 21 (2003) 1770.
[29] P. Serena, Optilux Toolbox. Available from: <www.optilux.sourceforge.net>.
[30] G. De Jonghe, M. Moeneclaey, Cycle-slip analysis of the Mth-power NDA feedforward carrier synchronizer for MPSK, Trans. Commun. 46 (1998) 1000.
[31] M.P. Fitz, Equivocation in nonlinear digital carrier synchronizers, Trans. Commun. 39 (1991) 1672.
[32] M.G. Taylor, Phase estimation methods for optical coherent detection using digital signal processing, J. Lightw. Technol. 27 (2009) 901.
[33] Y. Frignac, J.-C. Antona, S. Bigo, J.-P. Hamaide, Numerical optimization of pre- and in-line dispersion compensation in dispersion managed systems at 40 Gb/s, in: Proc. OFC '02, paper ThFF5.
[34] D. Wang, C.R. Menyuk, Polarization evolution due to Kerr nonlinearity and chromatic dispersion, J. Lightw. Technol. 17 (1999) 2520.
[35] P. Serena, A. Orlandini, A. Bononi, Scaling laws for weakly nonlinear WDM dispersion managed OOK systems, in: Proc. ECOC'06, paper We3.P.129, pp. 379–380.
[36] C. Weber, C.-A. Bunge, K. Petermann, Fiber nonlinearities in systems using electronic predistortion of dispersion at 10 and 40 Gbit/s, J. Lightw. Technol. 27 (2009) 3654.
[37] P. Serena, A. Orlandini, A. Bononi, Parametric gain approach to the analysis of single-channel DPSK/DQPSK systems with nonlinear phase noise, J. Lightw. Technol. 24 (2006) 2026.
[38] M. Jeruchim, Techniques for estimating the bit error rate in the simulation of digital communication systems, J. Sel. Areas. Commun. SAC-2 (1994) 153.
[39] J.-C. Antona, E. Greiller, A. Bononi, S. Petitreaud, S. Bigo, Revisiting binary sequence length requirements for the accurate emulation of highly dispersive transmission systems, in: Proc. ECOC'08, paper We.1.E.3.
[40] H. Kim, A.H. Gnauck, Experimental investigation of the performance limitation of DPSK systems due to nonlinear phase noise, Photon. Technol. Lett. 15 (2003) 320.
[41] J.C. Antona, S. Bigo, Physical design and performance estimation of heterogeneous optical transmission systems, C. R. Physique 9 (2008) 947.

Please cite this article in press as: A. Bononi et al., Nonlinear signal–noise interactions in dispersion-managed links with various modulation formats, Opt. Fiber Technol. (2009), doi:10.1016/j.yofte.2009.11.001

[42] A. Bononi, A. Vannucci, A. Orlandini, E. Corbel, S. Lanne, S. Bigo, Degree of polarization degradation due to cross-phase modulation and its impact on polarization mode dispersion compensators, J. Lightw. Technol. 21 (2003) 1903.
[43] M. Karlsson, H. Sunnerud, Effects of nonlinearities on PMD-induced system impairments, J. Lightw. Technol. 24 (2006) 4127.
[44] Q. Lin, G.P. Agrawal, Effects of polarization-mode dispersion on cross-phase modulation in dispersion-managed wavelength-division-multiplexed systems, J. Lightw. Technol. 22 (2004) 977.
[45] M. Winter, C.-A. Bunge, D. Setti, K. Petermann, A statistical treatment of cross-polarization modulation in DWDM systems, J. Lightw. Technol. 27 (2009) 3739.
[46] J. Renaudier et al., On the required number of WDM channels when assessing performance of 100 Gb/s coherent PDM-QPSK overlaying legacy systems, in: Proc. ECOC'09, paper 3.4.5.
[47] P. Serena, A. Bononi, Nonlinear phase noise mitigation by polarization mode dispersion in dispersion managed coherent PDM-QPSK Systems, in: Proc. ECOC'09, paper P4.12.
[48] E. Pincemin, A. Tan, A. Tonello, S. Wabnitz, J.D. Ania-Castañón, V. Mezenstev, S. Turitsyn, Y. Jaouün, L. Grüner-Nielsen, Performance comparison of 40 Gb/s ULH transmissions using CSRZ-ASK or CSRZ-DPSK modulation formats on UltraWave fiber TM fiber, Opt. Exp. 15 (2007) 11147.
[49] W. Hagmannn, J. Habermann, On the phase error distribution of an open loop phase estimator, in: Proc. ICC 1988, paper 32.5, pp. 1031–1037.

Please cite this article in press as: A. Bononi et al., Nonlinear signal–noise interactions in dispersion-managed links with various modulation formats, Opt. Fiber Technol. (2009), doi:10.1016/j.yofte.2009.11.001